

Connection between sea surface anomalies and atmospheric quasi-stationary waves

Article

Accepted Version

Wolf, G., Czaja, A., Brayshaw, D. J. ORCID: <https://orcid.org/0000-0002-3927-4362> and Klingaman, N. P. ORCID: <https://orcid.org/0000-0002-2927-9303> (2020) Connection between sea surface anomalies and atmospheric quasi-stationary waves. *Journal of Climate*, 33 (1). pp. 201-212. ISSN 1520-0442 doi: <https://doi.org/10.1175/JCLI-D-18-0751.1> Available at <https://centaur.reading.ac.uk/85868/>

It is advisable to refer to the publisher's version if you intend to cite from the work. See [Guidance on citing](#).

To link to this article DOI: <http://dx.doi.org/10.1175/JCLI-D-18-0751.1>

Publisher: American Meteorological Society

All outputs in CentAUR are protected by Intellectual Property Rights law, including copyright law. Copyright and IPR is retained by the creators or other copyright holders. Terms and conditions for use of this material are defined in the [End User Agreement](#).

www.reading.ac.uk/centaur

CentAUR

Central Archive at the University of Reading

Reading's research outputs online

1 **Connection between sea surface anomalies and atmospheric**
2 **quasi-stationary waves**

3 G. Wolf*

4 *Department of Meteorology, University of Reading, Reading, United Kingdom.*

5 *National Centre for Atmospheric Sciences, University of Reading, Reading, United Kingdom*

6 A. Czaja

7 *Imperial College, London, United Kingdom*

8 D.J. Brayshaw and N.P. Klingaman

9 *Department of Meteorology, University of Reading, Reading, United Kingdom.*

10 *National Centre for Atmospheric Sciences, University of Reading, Reading, United Kingdom*

11 *Corresponding author address: G. Wolf, Department of Meteorology, Earley Gate, University of
12 Reading, P.O. Box 243, Reading, Berkshire RG6 6BB, United Kingdom.

13 E-mail: g.a.wolf@reading.ac.uk

ABSTRACT

14 Large scale, quasi-stationary atmospheric waves (QSWs) are known to be
15 strongly connected with extreme events and general weather conditions. Yet,
16 despite their importance, there is still a lack of understanding about what
17 drives variability in QSW. This study is a step towards this goal, and identi-
18 fies three statistically significant connections between QSWs and sea surface
19 anomalies (temperature and ice cover) by applying a maximum covariance
20 analysis technique to reanalysis data (1979-2015). The two most dominant
21 connections are linked to the El Niño Southern Oscillation and the North At-
22 lantic Oscillation. They confirm the expected relationship between QSWs and
23 anomalous surface conditions in the tropical Pacific and the North Atlantic,
24 but they cannot be used to infer a driving mechanism or predictability from
25 the sea surface temperature or the sea ice cover to the QSW. The third con-
26 nection, in contrast, occurs between late winter to early spring Atlantic sea
27 ice concentrations and anomalous QSW patterns in the following late sum-
28 mer to early autumn. This new finding offers a pathway for possible long
29 term predictability of late summer QSW occurrence.

30 **1. Introduction**

31 Weather in mid-latitudes is typically associated with synoptic scale transient cyclones and anti-
32 cyclones, but occasionally more persistent weather regimes on scales of several days to about two
33 weeks can be observed (Horel 1985). These persistent weather regimes are often associated with
34 blocking highs at the jet exit regions (Masato et al. 2014) as part of a longitudinally extended
35 “quasi-stationary” wave (QSW, e.g. Nakamura et al. 1997; Wolf et al. 2018b).

36 QSWs are important because of their strong influence on weather and their link to extreme
37 events. Periods with increased QSW activity tend to be associated with more extremes, whereas
38 the absence of QSWs is linked to “near-average” weather (Screen and Simmonds 2014; Wolf
39 et al. 2018b). This connection between extreme events and mid-latitude wave patterns has been
40 suggested in several case studies (e.g. Petoukhov et al. 2016; Fragkoulidis et al. 2018) although
41 it is difficult to infer a general relationship from case studies alone (Screen and Simmonds 2013;
42 Petoukhov et al. 2013). Wolf et al. (2018b) showed the most dominant Northern Hemisphere QSW
43 patterns and the QSW patterns most relevant for European temperature extremes and anomalies
44 events and temperature anomalies, with strong correlations also to seasonal averages.

45 Despite the importance of QSWs, there is still a lack of understanding about possible large
46 scale drivers of the QSW variability. Most promising is the strong suggestion from literature that
47 large-scale low-frequency variability patterns, like El Niño Southern Oscillation (ENSO) or North
48 Atlantic Oscillation (NAO), can be linked to QSW patterns. Further, sea surface temperature (SST)
49 and sea ice concentration (SIC) anomalies seem to be linked to jet variability and therefore also to
50 QSW patterns.

51 ENSO may control the spatial and temporal variability of QSW activity of a full season, leading
52 to extreme events in North America (Trenberth and Guillemot 1996; Pan et al. 1999). It is well

53 known that a tropical heating source can lead to stationary anomalies in the general circulation
54 (Gill 1980), but its effects on non-stationary waves in mid-latitudes and teleconnections to extreme
55 events are less clear. Souders et al. (2014) have shown the anomalous wave pattern occurrence for
56 transient waves during La Niña and El Niño. Furthermore, the impact of ENSO on the Atlantic is
57 weaker and modulated by the Atlantic multidecadal oscillation, such that during its negative phase
58 the ENSO teleconnection is more apparent (Rodríguez-Fonseca et al. 2016).

59 In Europe, the NAO has a strong influence on temperature anomalies (Pozo-Vázquez et al. 2001)
60 and even strong droughts can be associated with the NAO phase (López-Moreno and Vicente-
61 Serrano 2008). To some extent, the NAO can be related to processes outside the Atlantic region,
62 connected by the presence of a wave. Jiang et al. (2017) showed that the Madden-Julian Oscil-
63 lation influences the behavior and persistence of NAO positive and negative phases. Feldstein
64 (2003) investigated the time evolution of the NAO associated with transients and QSWs, showing
65 a connection between the positive NAO and a preceding Pacific wavetrain.

66 The connection between sea ice anomalies and circulation changes are of particular importance,
67 because the persistence of sea ice anomalies makes them a possible source of seasonal to inter-
68 annual predictability. There is progress in understanding the connection between a changing cli-
69 mate and the tropospheric and stratospheric circulation response (e.g. review of Screen et al.
70 2018), but the impact of sea ice on mid-latitude waves in a changing climate is still uncertain and
71 widely discussed. Some studies conclude that stronger sea ice loss leads to decreased baroclinicity
72 which can lead to more persistent wave patterns (e.g. Overland et al. 2016), whereas other studies
73 link reduced sea ice with fewer planetary waves due to a weakening of the baroclinic-eddy wave
74 source (e.g. Smith et al. 2017). These discrepancies highlight the necessity to further investigate
75 and understand the atmospheric wave response to variability in sea surface temperatures and sea
76 ice. It is difficult to isolate the atmospheric response to changes in sea ice due to the many other in-

77 fluences on the atmospheric circulation, as well as a low signal-to-noise-ratio (Screen et al. 2014).
78 Regarding this aspect, Luo et al. (2019) highlighted the importance of the weakened north-south
79 gradient of background potential vorticity (PV) over Eurasia for Ural blocking and cold winters in
80 East Asia. The weakened PV gradient was linked therein to a warming climate and reduced sea
81 ice. The cold events, however, can also occur during a weakened PV gradient even without nega-
82 tive sea ice anomalies as a result of mid-latitude cold anomalies, but still only if there is blocking.
83 Such dependencies could be responsible for some of the above-mentioned discrepancies and the
84 difficulties to come to a clear conclusion.

85 Several studies link specific local changes in sea ice to impacts on the atmospheric circulation.
86 Wu et al. (2013) showed that above average winter sea ice concentrations west of Greenland can
87 lead to Atlantic SST anomalies persisting into spring, which feed back on the atmospheric sum-
88 mer circulation in northern Eurasia. Hall et al. (2017) showed that the Atlantic May SST tripole,
89 showing increased correlations with SST anomalies of the preceding months, can be associated
90 with the Atlantic jet speed in summer, while sea ice anomalies could also be related to a latitudinal
91 shift in the jet location. Petrie et al. (2015) found the Labrador sea ice concentration to be rele-
92 vant for the jet strength over North America, which affects north-western Europe via downstream
93 developing wave packets. Cause and effect between QSWs and sea ice anomalies is not always
94 obvious and should be considered with caution (Simmonds and Govekar 2014). For example, Sato
95 et al. (2014) linked anomalous sea ice retreats in the Barents-Kara sea to a shift in the Gulf Stream
96 front, leading to an atmospheric wave response with a teleconnection to the Arctic. These studies
97 further motivate investigating the connection between sea ice anomalies and QSW patterns.

98 The remainder of this paper is organized as follows. Section 2 presents the data and methods
99 used to calculate QSWs and to relate them to surface ocean anomalies (sea surface temperature
100 and sea ice concentrations). Results obtained by the application of the statistical method described

101 in section 2 are presented in section 3. Section 4 analyses the connection between late winter/early
102 spring sea surface anomalies and the associated QSW patterns in late summer/early autumn and
103 its possible physical connections. The key conclusions of this paper are summarized in section 5.

104 **2. Data and methods**

105 ERA-Interim reanalysis (Dee et al. 2011) is used for all meteorological quantities on a longitude-
106 latitude grid with $0.75^\circ \times 0.75^\circ$ resolution. The data are linearly detrended at each gridpoint over
107 1979 to 2015 for each season individually. This procedure allows us to focus on the intra-annual
108 connections between variables, without the effect of long term trends.

109 To identify the envelope field of the quasi-stationary waves (QSW) at 300 hPa we use the method
110 of Wolf et al. (2018b). The envelope field of the QSW is a phase independent, non-negative
111 measure of the waviness of the anomalous meridional wind, v' , in the zonal direction. We refer to
112 this envelope field as the amplitude of the QSW. The anomalous meridional wind is calculated as
113 $v' = \tilde{v} - \bar{\tilde{v}}$, where \tilde{v} is the 15-day lowpass filtered meridional wind - to remove faster transients -
114 and $\bar{\tilde{v}}$ is the daily climatology, to which we also applied a 15 day lowpass filter.

115 From this anomalous wind field, the phase-independent amplitude of the wave is calculated
116 using the method of Zimin et al. (2003). For this method a wavenumber range must be chosen,
117 which is assumed to represent the spatial scale of the waves of interest. In this study a wavenumber
118 range of about 4 to 8 in mid-latitudes is chosen, but instead of using a fixed wavenumber range,
119 a latitude-dependent wavenumber range is used, with a cosine decay towards higher latitudes,
120 following the maxima of the power spectra of the anomalous meridional wind v' (Wolf et al.
121 2018b, details therein)¹. The cosine weighting essentially leads to a latitude-independence of the

¹The data for the 12 hourly envelope fields of the quasi-stationary waves between 1 June 1979 and 31 August 2015, are available at the Centre for Environmental Data Analysis (Wolf et al. 2018a).

122 range of wavelengths, rather than of the wavenumbers. An advantage of the applied QSW method,
123 compared to other commonly used methods (such as Screen and Simmonds 2014; Kornhuber et al.
124 2017), is that it is a positive and phase independent measure of the wave packet in longitude-
125 latitude fields for one time-step. This allows to represent the spatial pattern of the investigated
126 wave packets and the application of time averages without having to deal with the problems of
127 phase cancellation (as it would be the case for time averages of anomalies of geopotential height
128 or meridional wind).

129 To identify statistical connections between QSWs and SST and SIC we apply a maximum co-
130 variance (MC) analysis between those variables, as described in Czaja and Frankignoul (2002).
131 The MC is calculated between monthly averaged anomaly fields. The anomalies are calculated as
132 the deviation from the climatological mean of the specific month. The regions used for the MC
133 analysis of the two variables are not necessarily the same and will be defined later. This method
134 identifies the modes that maximize the covariance between two possibly different variables, sim-
135 ilar to empirical orthogonal functions, which identify the modes that maximize the variance of
136 one variable in the underlying data. For investigating the covariance between different seasons,
137 monthly anomalies within each season are used. The term “season” refers to a period of any three
138 consecutive months. Introducing further a time lag for one of the variables identifies potentially
139 causal relationships. To give similar weight to each season, the anomalies are further normalized
140 by the standard deviation of the specific variables in the specific season. To identify the relevance
141 of specific modes, a Monte Carlo approach is applied to determine if the modes are statistically
142 significant. The method is therefore a purely statistical approach to connect variables in the under-
143 lying data; it does not include any information about the nature of possible physical connections.
144 For the MC analysis of two variables in different seasons, the Monte Carlo approach repeats the
145 MC calculation 1000 times (if not stated otherwise) by holding the first variable fixed, but ran-

146 domly permutating the years for the second variable. The permutation is, however, only applied to
147 each season as a whole. This means that consecutive months within one season in the MC analysis
148 are preserved in the Monte Carlo approach; only the years are shuffled. It is important to realize
149 that the results of the MC analysis cannot by themselves be used as proof of causality, even when
150 strong lead/lag relationships are found between variables. Instead, MCA analysis is used here to
151 identify potential causal patterns in order to stimulate the further investigations required to identify
152 physical causal processes.

153 To represent sea surface anomalies, we combine the fields of SST and SIC into one matrix, be-
154 fore applying the MC analysis. To do so, both fields are normalized by their seasonal standard
155 deviation, using all gridpoints at which anomalies could be observed in the dataset for the asso-
156 ciated season. For SIC, this includes all gridpoints inside the maximum areal extent of SIC in
157 the dataset. The combined matrix is created by concatenating both normalized matrices along the
158 latitude dimension. The MC analysis then proceeds as usual by assuming that the combined field
159 represents one variable. In the following, we will refer to the combined field as SSTSIC. The MC
160 patterns using either SST or SIC individually are qualitatively very similar. In case of a difference
161 to the combined SSTSIC, this will be highlighted in the text. Note that the technique is linear so
162 that the signs of patterns shown in the figures below can be reversed (the relative signs between
163 QSW and SSTSIC remaining unchanged).

164 The values for the global pattern indices used in this study, namely the North Atlantic Os-
165 cillation (NAO) and the El Niño Southern Oscillation in the Niño 3.4 region (Niño 3.4), are
166 retrieved from the CPC database of the National Oceanic and Atmospheric Administration
167 (<http://www.cpc.ncep.noaa.gov>).

168 **3. Connection between ocean anomalies and QSWs**

169 In this section we identify connections between anomalous QSW amplitudes and anomalies in
170 SSTSIC using monthly averages. We do this by applying the MC analysis between those two
171 variables, as described in section 2, for various regions and with lags between -6 and $+9$ months
172 (QSW leads surface variables at negative lags). Results are shown in Fig. 1a (extended Northern
173 Hemisphere SSTSIC anomalies) and Fig. 2a (Atlantic SSTSIC anomalies). These figures display
174 in colour the squared covariance of the leading MC mode between QSW and SSTSIC as a function
175 of season and time lag, following Czaja and Frankignoul (2002, their Fig. 1). For example in
176 Fig. 1a, large squared covariances are found when SSTSIC is taken in NDJ (x-axis) and QSW two
177 months later (JFM, white rectangle highlighted). It is worth noting that the largest synchronous
178 values occur during the colder seasons. Statistical significance is indicated by the green plusses
179 in these plots while the contours display the correlation coefficient between large scale modes of
180 climate variability and the QSW leading mode timeseries. Application of this procedure reveals
181 three statistically significant connections which are discussed in the following three subsections.

182 *a. Connection between QSWs and El Niño Southern Oscillation*

183 High covariances for the first MC mode between extended Northern Hemisphere SSTSIC (20°S
184 to 85°N) and extratropical Northern Hemisphere QSWs (30°N to 85°N) in Fig. 1a identify strong
185 lead/lag connections between those variables for all seasons. The connection for all seasons can
186 be understood by a persistent SSTSIC anomaly from the warmer seasons into the colder seasons
187 (strong covariances along the diagonal line from top left to bottom right in Fig. 1a) with strong
188 QSW anomalies manifesting only during the colder seasons. Due to the persistence of these
189 increased covariances, the covariances during summer with large positive lags are also potentially
190 physically meaningful, although not statistically significant. Since the statistically significant co-

191 variances (green dots and plusses) occur in an area of the plot which does show high correlations
192 between the time series of the principal component of QSW and the Niño 3.4 index (black con-
193 tours in Fig. 1a), we can associate this connection to El Niño Southern Oscillation (ENSO). Since
194 this connection represents the clear first mode in the MC analysis, ENSO can be identified, on a
195 hemispheric scale, as the dominant oceanic anomaly associated with QSW variability.

196 The diagonal tilting of the statistically significant covariances in Fig. 1a along a straight line
197 indicates that this connection exists for QSW patterns mainly from DJF to FMA. Due to the con-
198 nection to ENSO with the strongest anomalies in the tropical Pacific, it is not surprising that this
199 specific connection is dominated by the SST contribution and cannot be reproduced by using SIC
200 only (not shown).

201 The associated latitude-longitude pattern of the MC mode between SSTSIC in NDJ and QSW
202 amplitudes in JFM (lag of +2 months, white box in Fig. 1a) shows increased QSW amplitudes
203 over the Pacific, North America and the subtropical Atlantic and decreased QSW amplitudes over
204 Europe and the high-latitude North Atlantic during La Niña (Fig. 1b, continuous and dashed con-
205 tours, respectively - the La Niña state is clearly seen in the SST anomaly pattern shown in colour
206 in Fig. 1b). Due to the linearity of the MC analysis, the exact opposite is true for El Niño (flipped
207 signs for both SSTSIC and QSW). The patterns for the statistically significant covariances at pos-
208 itive lags are very similar, whereas for negative lags this is less clear (not shown here). Due to
209 the long persistence of SST anomalies during ENSO phases of either sign and the statistical sig-
210 nificance occurring at both positive and negative lags, it is impossible to deduce a direct forcing
211 of QSW variability by the SST pattern in Fig. 1. Modeling work is necessary to understand how
212 such strong covariances come about, perhaps through an atmospheric bridge (Lau and Nath 1994;
213 Alexander et al. 2002). The connection between the ENSO SST pattern and QSW therefore sug-
214 gests predictive skill for the QSW insofar as the ENSO SST pattern in itself tends to be strongly

215 persistent (thus a month with warm SSTs tends to be followed by another warm SST month, con-
216 sistent with similar QSW patterns being observed in both). This should not, however, be taken
217 to imply a direct causal connection between ENSO SSTs and remote QSW anomalies at some
218 later time. A seasonal forecast model that skillfully predicted the persistence for ENSO might also
219 skillfully predict the preferred QSW pattern, but such an investigation is outside the scope of this
220 paper.

221 *b. Connection between QSWs and North Atlantic Oscillation*

222 Using again the same region for the QSW amplitudes (30°N to 85°N), but reducing the region
223 for the SSTSIC to the North Atlantic north of 20°N (80°W to 40°E), the first MC mode shows
224 strong covariances associated with negative lags (Fig. 2a, i.e. QSW leads SSTSIC). These covari-
225 ances are associated with the NAO (blue contour lines). The statistically significant covariances at
226 negative lags suggest that the NAO-related SSTSIC pattern is reflecting a forcing of the ocean by
227 the atmosphere, consistent with previous studies (e.g. Czaja and Frankignoul 2002; Visbeck et al.
228 2003). For the phase shown in Fig.2b, it consists of a tripolar SST anomaly, with colder conditions
229 along the separated Gulf Stream sandwiched between anomalously warm conditions to the north
230 and south (colours). The SIC pattern is, in response to a negative NAO phase, less sea ice in the
231 Labrador sea (green contours) and more sea ice in the Greenland-Barents Sea (magenta contours).

232 The associated wave pattern (Fig. 2b, based on the lags/month highlighted by white box at
233 negative lags in Fig. 2a) represents a reduction of wave amplitude over 30°N and an enhancement
234 poleward of 50°N. It was shown to be associated with cold temperatures at 850 hPa in Central
235 Europe (Wolf et al. 2018b), agreeing with previous results for temperature anomalies associated
236 with the negative phase of the NAO (Pozo-Vázquez et al. 2001). The shift between the strongest
237 covariances and highest correlation in Fig. 2a is the result of an evolving QSW pattern, from mid-

238 latitudes towards high latitudes and a further shift from the Pacific towards the Atlantic (not shown
239 here). Only the pattern at the later stage of this evolving QSW signal (Fig. 2b) is strongly correlated
240 with the NAO, which is the reason for the reduced correlations occurring for the preceding seasons.
241 However, the associated SST pattern is consistent and shows for all negative lags the typical NAO-
242 like Atlantic SST-tripole (as the one in Fig. 2b) and therefore are those QSW patterns also expected
243 to be associated with the NAO. As for the connection to ENSO, this connection is also associated
244 dominantly with QSW anomalies during winter and the adjacent months. In winter, ENSO and
245 NAO show strong correlations with the first three EOFs of Northern hemispheric QSW amplitudes
246 (Wolf et al. 2018b), which highlights again the importance of these two QSW patterns.

247 *c. Connection between QSWs and North Atlantic high latitude surface ocean anomalies*

248 Besides the dominant two connections with ENSO or the NAO, we identified a third significant
249 connection through MC analysis between late winter to early spring SSTSIC and late summer to
250 early autumn QSW amplitudes (second white box in Fig. 2a, i.e. SSTSIC in FMA leads QSW by
251 about 5 months).

252 The associated latitude-longitude QSW pattern in JAS shows increased mid-latitude and de-
253 creased high latitude QSW amplitudes (Fig. 2c), covarying with the SST tripole and SIC anomalies
254 described above. That is, we find a very similar SSTSIC pattern but associated at lag +5 months
255 with a generally opposing QSW pattern than found at lag -1 month (i.e., the signs of the anomaly
256 in the high and mid-latitude regions are reversed). Note that the lags of +4 and +6 months show
257 a consistent QSW pattern (not shown). In addition, the same statistically significant pattern can
258 be reproduced using only SST or only SIC for the MC analysis, instead of the combined SSTSIC
259 field (not shown here).

260 The pattern of increased mid-latitude QSW amplitudes in summer (Fig. 2c) is linked to strong
261 lower troposphere temperature anomalies of either sign (but mainly warm anomalies) over Central
262 Europe (Wolf et al. 2018b). QSW composites associated with extreme warm anomalies in the
263 same region showed a very similar wave pattern. Further, cold anomalies in Central Europe were
264 associated with preceding increased high latitude QSW activity. This suggests that the QSW
265 patterns, related to European temperature anomalies in summer could be linked to Atlantic SSTSIC
266 anomalies in late winter to early spring.

267 A further separation of the SSTSIC region into northern and southern parts (20°N to 60°N and
268 60°N to 85°N) reveals that the MC analysis for the northern part leads to statistically significant
269 covariances, whereas MC analysis for the southern part does not (not shown here; see section 4
270 below for more sensitivity tests of the MC analysis). The associated longitude-latitude patterns
271 for the northern part are very similar to the ones using the full Atlantic region (20°N to 85°N).
272 This suggests the importance of high latitude sea surface anomalies for this connection, but the
273 associated longitude-latitude patterns for the southern part show similarities to the ones for the
274 northern part, at least for lags of +5 and +6 months, meaning that the southern part is not nec-
275 essarily irrelevant for this teleconnection. The role of the SIC in this connection is investigated
276 further in section 4.

277 To check the robustness of this connection between FMA SSTSIC and subsequent JAS QSW
278 amplitudes, we calculated composite FMA SSTSIC anomalies for the 8 JAS seasons with the
279 strongest QSW anomalies in mid- (225°W to 45°E, 40°N to 60°N: 1987, 1985, 1998, 1981, 2003,
280 2007, 1986 and 1995) and high latitudes (North of 65°N: 1984, 1995, 1993, 1979, 2008, 1991,
281 1983 and 2004), where the years given in brackets are ordered by their intensity, starting with
282 the highest intensity. The resulting SSTSIC patterns are very similar to the one given in Fig. 2c
283 (not shown). The results are not sensitive to the number of seasons used for the composite. This

284 supports the hypothesis of a connection between SSTSIC in FMA and QSW amplitudes in the
285 following JAS. We now briefly investigate possible physical mechanisms for this connection.

286 **4. Possible physical links for the inter-seasonal ocean and QSW connection**

287 In the previous section we have already shown the importance of the high-latitude Atlantic for
288 the connection between late winter/early spring SSTSIC anomalies and late summer/early autumn
289 QSW amplitude anomalies. Using only SIC for the MC analysis leads to more statistically signif-
290 icant signals of the same patterns for neighbouring seasons with similar lags (Fig. S1), additional
291 to the previously found statistically significant signal at a lag of +5 months for FMA by using
292 SST only or SSTSIC (Fig. 2a). From this we can hypothesize that SIC is the main contributor
293 to this connection. Such SIC anomalies, if persistent enough, could interact with the large scale
294 atmospheric circulation by modifying the baroclinicity, acting on similar sub-annual timescales as
295 in previous studies (e.g. Wu et al. 2013). We possibly see an atmospheric response in summer
296 and not spring, because of the importance of the jet location relative to the region of the modified
297 baroclinicity. The center (defined by the peak intensity) of the lower tropospheric jet at 850 hPa
298 in the Atlantic jet entry region may still be too far south in April to June (climatological value at
299 42°N, between 60°W and 30°W), whereas in July to September it shifts northward (climatological
300 value at 49°N). This means that the change in baroclinicity by the higher-latitude ocean anoma-
301 lies close to the Labrador Sea in April to June do not align well with the jet position in the West
302 Atlantic, which therefore does not optimally contribute as a baroclinic energy source for further
303 wave amplification. This could change, once the climatological jet location moves towards higher
304 latitudes in the following months. As discussed in the introduction, this source of energy could
305 be a relevant mechanism for wave amplification (e.g. Smith et al. 2017). How this interaction

306 works clearly needs further investigation but the statistical result reported here appears robust. We
307 proceed below to further analysis of the empirical relationship captured in Fig. 2c.

308 To interact with the late summer atmospheric circulation, the late winter SIC anomalies must
309 be persistent enough. To check the persistence of these SIC anomalies, we calculate a lag com-
310 posite of area-averaged SST and SIC anomalies in the Greenland-Barents Sea (0°E to 60°E , 50°N
311 to 80°N) and Labrador Sea (70°W to 50°W , 50°N to 65°N) for the 8 seasons with the strongest
312 positive and negative SIC differences between those two regions in FMA (Fig. 3a). As a reminder,
313 those regions are chosen to cover the relevant SIC anomalies for the investigated connection in
314 this section (see Fig. 2b and c). We refer to this difference as I_{diff} . Positive values indicate more
315 anomalous sea ice in the Greenland-Barents Sea than in the Labrador Sea. All composite anoma-
316 lies (SST and SIC) for positive I_{diff} (solid lines) and negative I_{diff} (dashed lines) show the same sign
317 until JAS. This persistence is insensitive to the number of seasons used for the composite. If these
318 anomalies are optimally aligned to interact with the wave guide in summer, this could cause the
319 anomalous QSW patterns in summer.

320 Similar to the previous test of robustness, we calculate the QSW patterns in JAS for the years
321 with the strongest positive (1979, 2011, 2010, 1981, 1998, 1987, 2004 and 2003) and negative
322 values (1984, 1993, 1983, 1990, 1992, 1991, 1995 and 2014) for I_{diff} . As expected from the results
323 of the MC analysis, the composite for the years with negative I_{diff} values leads to anomalously strong
324 high latitude QSW amplitudes (Fig. 3b), exceeding the 99th percentile (white dots). The composite
325 for the years with positive I_{diff} values leads to anomalous strong and statistically significant mid-
326 latitude QSW amplitudes (Fig. 3c), although there is a gap of increased QSW amplitudes over
327 North America. But overall, the sign of I_{diff} clearly leads to a separation of the QSW patterns with
328 strong values at high or mid-latitudes. The qualitative results are insensitive to the exact choice of
329 the regions used to calculate I_{diff} , as long as they capture the dipole character of this anomaly.

330 Comparing the SSTSIC in Fig. 2b and 2c reveals very similar patterns. This suggests that the
331 NAO, which is strongly associated with the QSW and SST pattern of Fig. 2b, represents the com-
332 mon feature behind both connections (the ones shown in Fig. 2b and Fig. 2c). The associated
333 SSTSIC pattern found for both connections therefore appears to link the two atmospheric anoma-
334 lies in autumn/winter and the following summer/autumn. This would mean that the autumn/winter
335 QSW pattern leads to a specific late winter/spring SSTSCI pattern which further leads to a specific
336 QSW pattern in late summer/early autumn. In the following we will provide further support for
337 this hypothesis. First for the connection between winter NAO index and the following late sum-
338 mer/early autumn QSW anomalies. For this connection we obtain a linear correlation of -0.42
339 between mid-latitude (225°W to 45°E and 40°N to 60°N) averaged QSW amplitudes in JAS and
340 the averaged NAO value in the preceding DJF (Fig. S2a), whereas strong high-latitude (north of
341 65°N) averaged QSW amplitudes in JAS seem to occur mainly after a positive NAO in the pre-
342 ceding DJF (Fig. S2b). Second, if the above hypothesis is true, one can possibly expect increased
343 covariances between similar QSW patterns in autumn/winter and the following summer/autumn.
344 To test this we repeated the MC analysis of Fig. 2a between extratropical Northern Hemisphere
345 QSW amplitudes and QSW amplitudes limited to the Atlantic basin (instead of SSTSIC limited
346 to the Atlantic basin). The QSW amplitudes in the second region are restricted to the Atlantic
347 basin, because of the known strong connection between Atlantic QSW anomalies and the NAO
348 (Wolf et al. 2018b, or Fig. 2a and 2b herein). This MC analysis indeed shows a statistically signif-
349 icant connection between autumn to winter Atlantic QSW amplitudes and Northern Hemisphere
350 QSW amplitudes with about a $+7$ month lag, which further show increased correlations with NAO
351 (Fig. S3). Because of the strong atmospheric internal variability and its nonlinear behaviour, the
352 presented linear statistical method does not prove this hypothesis, but supports the potential for
353 recurrent interactions between QSWs, SST and SIC anomalies between autumn to winter and late

354 summer to early autumn. To clarify the details of these recurrent interactions, further analysis is
355 necessary.

356 **5. Conclusion and discussion**

357 In a previous study (Wolf et al. 2018b) we showed the connection between QSWs and European
358 weather and extreme events and identified the main modes of QSW variability. We highlighted
359 therein the importance of better understanding the physical mechanisms underlying these QSW
360 patterns and their variability. This analysis represents the first step towards this goal by investigat-
361 ing the link between surface ocean anomalies and QSW amplitudes with lags of several months.
362 Therefore, we use the MC analysis as a powerful tool to identify statistical connections between
363 different variables, as done in previous studies (e.g. Czaja and Frankignoul 2002; Frankignoul
364 et al. 2014).

365 We identified three statistical significant connections between sea surface anomalies and anoma-
366 lous QSW amplitudes. The two most dominant connections occur during the colder seasons (late
367 autumn, winter, early spring) and can be related to ENSO and NAO. These global pattern indices
368 are not only linked to strong temperature anomalies and extreme events (e.g. Pan et al. 1999;
369 Pozo-Vázquez et al. 2001; López-Moreno and Vicente-Serrano 2008), but they can also be asso-
370 ciated with some predictability (Latif et al. 1998; Scaife et al. 2014). It is therefore important to
371 understand the evolution of the associated QSW patterns, which are more directly linked to the as-
372 sociated weather and therefore can help to get a deeper understanding of the evolution of extremes
373 or why predictability increases in remote regions. This is no contradiction with the previous state-
374 ment that our results for the ENSO connection cannot be used to infer predictability for the QSWs.
375 The results from the applied statistical method could only be used to highlight the general con-
376 nection between the SST associated with ENSO and mid-latitude QSWs. The QSW pattern itself

377 indicates possible teleconnection regions, but to understand the details of the teleconnections or
378 the time evolution and frequency of the QSWs during an ENSO event, further analysis beyond this
379 monthly lagged analysis is needed. During La Niña we identified an increase in QSW amplitudes
380 over the North Pacific and North America, reaching downstream into the subtropical Atlantic to-
381 wards the Mediterranean, whereas over the high-latitude North Atlantic and Europe a decrease
382 in QSW amplitudes can be observed. For the Atlantic SST tripole, associated with the negative
383 NAO phase, QSW amplitudes show increased values at high latitudes with a maximum over the
384 Atlantic and a slight decrease along the subtropical Asian jet. This connection exists for QSW
385 amplitudes with negative lags in the MC analysis, suggesting the SST tripole to be an imprint of
386 the preceding atmospheric flow pattern. This dominant atmosphere-driving-ocean relationship is
387 in agreement with previous studies (e.g. Czaja and Frankignoul 2002; Visbeck et al. 2003). These
388 QSW patterns, associated with NAO and ENSO, explain a large contribution of the overall QSW
389 variability during the cold season. The focus in that paragraph, concerning the global pattern in-
390 dices, was towards La Niña and the negative NAO phase. Due to the linearity of the MC analysis,
391 the exact opposite is true for El Niño or the positive NAO (reversed signs for both SSTSIC and
392 QSW, relative signs remain unchanged).

393 The third statistical significant connection between those two variables occurs between FMA
394 Atlantic high latitude sea surface anomalies and JAS extratropical Northern Hemisphere QSW
395 anomalies. We identified the SIC as the main contributor to this connection. The large lag of
396 about +5 months can possibly be attributed to the persistence of the associated SIC pattern. We
397 showed that for years with a strong anomaly of such a SIC pattern in FMA, this anomaly persists
398 into JAS. Interacting with the general circulation, these sea ice anomalies could be responsible for
399 the QSW response in the following late summer/early autumn. The reason why this interaction is
400 not apparent during late spring/early summer could be that the locations between the baroclinic

401 modified region by the SIC or associated SST anomalies and the wave guide for the QSWs are not
402 optimally aligned. How this interaction works in detail needs further investigation.

403 Our results about the FMA SSTSIC anomalies show strong similarities with the findings of
404 Frankignoul et al. (2014), in which they showed that the Atlantic SIC anomalies in the Labrador
405 sea and Greenland-Barents Sea (they refer to it as “seesaw” pattern) during late winter/early spring
406 can be associated to preceding NAO anomalies and which by itself leads to a NAO-like pattern
407 of opposite polarity about 6 weeks later. This suggests the same underlying driving mechanism
408 between winter NAO and FMA SSTSIC anomalies, but distinct to the analysis of Frankignoul
409 et al. (2014), we identified a longer lag connection between their “seesaw” pattern and upper
410 tropospheric QSWs in JAS. In agreement with our findings, they also identified SIC anomalies as
411 the main contributor to this connection. They further discussed that including the North Pacific SIC
412 dipole pattern of negative and positive anomalies in the Bering and Okhotsk Sea, which appears
413 also in our findings (see Fig. 2c), increases the statistical significance.

414 To test the robustness of the results, we included a composite analysis, showing the same sea
415 surface or QSW patterns as for the linear MC analysis by applying a ± 5 months lag to each of the
416 composited variables separately. This further increases the confidence in the findings of the applied
417 statistical analysis. Due to the findings of the connection between NAO and QSW anomalies
418 in autumn to winter, the connection between winter NAO and FMA SSTSIC anomalies and the
419 connection between FMA SSTSIC anomalies and JAS QSW anomalies, we hypothesized that a
420 connection between autumn to winter QSWs and QSWs in the following JAS may be apparent.
421 Repeating the MC analysis for QSW amplitudes between different seasons does indeed show
422 increased covariances, supporting this hypothesis.

423 These results are all based on the first MC modes for the different regions or variables, to high-
424 light the most dominant and robust signals. Higher MC modes also include some statistically

425 significant signals, but those are fewer and less coherent. The second MC modes show mainly
426 two statistically significant signals. For SSTSIC in the extratropical Northern Hemisphere (first
427 mode given in Fig. 1a) the area of the statistically significant covariances is very similar to the one
428 found for negative lags in Fig. 2a, also with increased correlations with the winter NAO index,
429 meaning that the second MC mode for extratropical Northern Hemisphere SSTSIC describes the
430 same signal as the first MC mode for SSTSIC in the Atlantic region. The second MC mode for
431 SSTSIC in the Atlantic shows statistically significant signals in spring to summer, with a lag of
432 about +4 months. The SSTSIC signal is represented again by the previously discussed NAO-like
433 imprint. The associated QSW patterns are also partly very similar to the signal found for FMA
434 with a +5 lag, suggesting that the previously identified SSTSIC not only appears in late winter, but
435 also into spring and summer. The patterns are less coherent, however, and besides the very similar
436 QSW pattern we can also identify a similar SSTSIC pattern, but which is associated with a east-
437 west dipole in QSW amplitudes, with positive anomalies towards Europe and negative over North
438 America for a negative NAO. This second mode could explain the gap of increased mid-latitude
439 QSW amplitudes in the composite study (Fig. 3c).

440 In this paper we were able to link some important QSW patterns to surface ocean anomalies.
441 Due to the more direct link of the QSW patterns to the associated weather, compared to the use of
442 global pattern indices, their consideration can be helpful in the understanding and interpretation
443 of specific teleconnection patterns. We further demonstrated the relevance of SIC anomalies on
444 the QSW patterns of following seasons, which can be very helpful for long term predictability of
445 large scale weather conditions or the occurrence of extremes.

446 *Acknowledgments.* We acknowledge funding from the Natural Environment Research Council
447 (NERC) for the ODYSEA project (grant number: NE/M006085/1). Nicholas P. Klingaman was
448 funded by a NERC Independent Research Fellowship (NE/L010976/1).

449 **References**

450 Alexander, M. A., I. Blad, M. Newman, J. R. Lanzante, N.-C. Lau, and J. D. Scott, 2002: The
451 atmospheric bridge: The influence of enso teleconnections on airsea interaction over the global
452 oceans. *Journal of Climate*, **15** (16), 2205–2231, doi:10.1175/1520-0442(2002)015<2205:
453 TABTIO>2.0.CO;2.

454 Czaja, A., and C. Frankignoul, 2002: Observed impact of atlantic sst anomalies on the north
455 atlantic oscillation. *J. Climate*, **15** (6), 606–623, doi:10.1175/1520-0442(2002)015<0606:
456 OIOASA>2.0.CO;2.

457 Dee, D. P., and Coauthors, 2011: The era-interim reanalysis: configuration and performance of
458 the data assimilation system. *Quart. J. Roy. Meteor. Soc.*, **137** (656, A), 553–597, doi:10.1002/
459 qj.828.

460 Feldstein, S. B., 2003: The dynamics of nao teleconnection pattern growth and decay. *Quart. J.*
461 *Roy. Meteor. Soc.*, **129** (589), 901–924, doi:10.1256/qj.02.76.

462 Fragkoulidis, G., V. Wirth, P. Bossmann, and A. H. Fink, 2018: Linking northern hemisphere
463 temperature extremes to rossby wave packets. *Quart. J. Roy. Meteor. Soc.*, **144** (711), 553–566,
464 doi:10.1002/qj.3228.

465 Frankignoul, C., N. Sennéchaël, and P. Cauchy, 2014: Observed atmospheric response to
466 cold season sea ice variability in the arctic. *J. Climate*, **27** (3), 1243–1254, doi:10.1175/
467 JCLI-D-13-00189.1.

- 468 Gill, A. E., 1980: Some simple solutions for heatinduced tropical circulation. *Quart. J. Roy. Meteor. Soc.*, **106 (449)**, 447–462, doi:10.1002/qj.49710644905.
- 469
- 470 Hall, R. J., J. M. Jones, E. Hanna, A. A. Scaife, and R. Erdélyi, 2017: Drivers and potential
471 predictability of summer time north atlantic polar front jet variability. *Climate Dyn.*, **48 (11)**,
472 3869–3887, doi:10.1007/s00382-016-3307-0.
- 473 Horel, J. D., 1985: Persistence of the 500 mb height field during northern hemisphere winter. *Mon.*
474 *Wea. Rev.*, **113 (11)**, 2030–2042, doi:10.1175/1520-0493(1985)113<2030:POTMHF>2.0.CO;2.
- 475 Jiang, Z., S. B. Feldstein, and S. Lee, 2017: The relationship between the maddenjulian oscillation
476 and the north atlantic oscillation. *Quart. J. Roy. Meteor. Soc.*, **143 (702)**, 240–250, doi:10.1002/
477 qj.2917.
- 478 Kornhuber, K., V. Petoukhov, D. Karoly, S. Petri, S. Rahmstorf, and D. Coumou, 2017: Summer-
479 time planetary wave resonance in the northern and southern hemispheres. *J. Climate*, **30 (16)**,
480 6133–6150, doi:10.1175/JCLI-D-16-0703.1.
- 481 Latif, M., and Coauthors, 1998: A review of the predictability and prediction of enso. *Journal of*
482 *Geophysical Research: Oceans*, **103 (C7)**, 14 375–14 393, doi:10.1029/97JC03413.
- 483 Lau, N.-C., and M. J. Nath, 1994: A modeling study of the relative roles of tropical and extratrop-
484 ical sst anomalies in the variability of the global atmosphere-ocean system. *Journal of Climate*,
485 **7 (8)**, 1184–1207, doi:10.1175/1520-0442(1994)007<1184:AMSOTR>2.0.CO;2.
- 486 López-Moreno, J. I., and S. M. Vicente-Serrano, 2008: Positive and negative phases of the win-
487 tertime north atlantic oscillation and drought occurrence over europe: A multitemporal-scale
488 approach. *J. Climate*, **21 (6)**, 1220–1243, doi:10.1175/2007JCLI1739.1.

- 489 Luo, D., X. Chen, J. Overland, I. Simmonds, Y. Wu, and P. Zhang, 2019: Weakened potential
490 vorticity barrier linked to recent winter arctic sea ice loss and midlatitude cold extremes. *Journal*
491 *of Climate*, **32** (14), 4235–4261, doi:10.1175/JCLI-D-18-0449.1.
- 492 Masato, G., T. Woollings, and B. J. Hoskins, 2014: Structure and impact of atmospheric blocking
493 over the euro-atlantic region in present-day and future simulations. *Geophys. Res. Lett.*, **41** (3),
494 1051–1058, doi:10.1002/2013GL058570.
- 495 Nakamura, H., M. Nakamura, and J. Anderson, 1997: The role of high- and low-frequency dynam-
496 ics in blocking formation. *Mon. Wea. Rev.*, **125** (9), 2074–2093, doi:10.1175/1520-0493(1997)
497 125<2074:TROHAL>2.0.CO;2.
- 498 North, G., T. Bell, R. Cahalan, and F. Moeng, 1982: Sampling errors in the estimation of em-
499 pirical orthogonal functions. *Mon. Wea. Rev.*, **110** (7), 699–706, doi:10.1175/1520-0493(1982)
500 110<0699:SEITEO>2.0.CO;2.
- 501 Overland, J., and Coauthors, 2016: Nonlinear response of mid-latitude weather to the changing
502 arctic. *Nature Climate Change*, **6**, 992–999, doi:10.1038/NCLIMATE3121.
- 503 Pan, Z., M. Segal, R. Arritt, T. Chen, and S. Weng, 1999: A method for simulating effects of
504 quasi-stationary wave anomalies on regional climate. *J. Climate*, **12** (5, 1), 1336–1343, doi:
505 10.1175/1520-0442(1999)012<1336:AMFSEO>2.0.CO;2.
- 506 Petoukhov, V., S. Petri, S. Rahmstorf, D. Coumou, K. Kornhuber, and H. J. Schellnhuber, 2016:
507 Role of quasiresonant planetary wave dynamics in recent boreal spring-to-autumn extreme
508 events. *Proc. Natl. Acad. Sci. (USA)*, **113** (25), 6862–6867, doi:10.1073/pnas.1606300113.

509 Petoukhov, V., S. Rahmstorf, S. Petri, and H. J. Schellnhuber, 2013: Reply to screen and
510 simmonds: From means to mechanisms. *Proceedings of the National Academy of Sciences*,
511 **110 (26)**, E2328–E2328, doi:10.1073/pnas.1305595110.

512 Petrie, R. E., L. C. Shaffrey, and R. T. Sutton, 2015: Atmospheric response in summer linked to
513 recent arctic sea ice loss. *Quart. J. Roy. Meteor. Soc.*, **141 (691)**, 2070–2076, doi:10.1002/qj.
514 2502.

515 Pozo-Vázquez, D., M. J. Esteban-Parra, F. S. Rodrigo, and Y. Castro-Díez, 2001: A study of nao
516 variability and its possible non-linear influences on european surface temperature. *Climate Dyn.*,
517 **17 (9)**, 701–715, doi:10.1007/s003820000137.

518 Rodríguez-Fonseca, B., and Coauthors, 2016: A review of enso influence on the north atlantic. a
519 non-stationary signal. *Atmosphere*, **7 (7)**, doi:10.3390/atmos7070087.

520 Sato, K., J. Inoue, and M. Watanabe, 2014: Influence of the gulf stream on the barents sea ice re-
521 treat and eurasian coldness during early winter. *Environmental Research Letters*, **9 (8)**, 084 009,
522 doi:10.1088/1748-9326/9/8/084009.

523 Scaife, A. A., and Coauthors, 2014: Skillful longrange prediction of european and north american
524 winters. *Geophys. Res. Lett.*, **41 (7)**, 2514–2519, doi:10.1002/2014GL059637.

525 Screen, J. A., T. J. Bracegirdle, and I. Simmonds, 2018: Polar climate change as manifest
526 in atmospheric circulation. *Current Climate Change Reports*, **4 (4)**, 383–395, doi:10.1007/
527 s40641-018-0111-4.

528 Screen, J. A., C. Deser, I. Simmonds, and R. Tomas, 2014: Atmospheric impacts of arctic sea-
529 ice loss, 1979–2009: separating forced change from atmospheric internal variability. *Climate*
530 *Dynamics*, **43 (1)**, 333–344”, doi:10.1007/s00382-013-1830-9.

531 Screen, J. A., and I. Simmonds, 2013: Caution needed when linking weather extremes to amplified
532 planetary waves. *Proceedings of the National Academy of Sciences*, **110** (26), E2327–E2327,
533 doi:10.1073/pnas.1304867110.

534 Screen, J. A., and I. Simmonds, 2014: Amplified mid-latitude planetary waves favour particular
535 regional weather extremes. *Nature Climate Change*, **4** (8), 704–709, doi:10.1038/nclimate2271.

536 Simmonds, I., and P. D. Govekar, 2014: What are the physical links between arctic sea ice loss
537 and eurasian winter climate? *Environmental Research Letters*, **9** (10), 101 003, doi:10.1088/
538 1748-9326/9/10/101003.

539 Smith, D. M., N. J. Dunstone, A. A. Scaife, E. K. Fiedler, D. Copey, and S. C. Hardiman, 2017:
540 Atmospheric response to arctic and antarctic sea ice: The importance of oceanatmosphere cou-
541 pling and the background state. *J. Climate*, **30** (12), 4547–4565, doi:10.1175/JCLI-D-16-0564.
542 1.

543 Souders, M. B., B. A. Colle, and E. K. M. Chang, 2014: The climatology and characteristics
544 of rossby wave packets using a feature-based tracking technique. *Mon. Wea. Rev.*, **142** (10),
545 3528–3548, doi:10.1175/MWR-D-13-00371.1.

546 Trenberth, K., and C. Guillemot, 1996: Physical processes involved in the 1988 drought and 1993
547 floods in north america. *J. Climate*, **9** (6), 1288–1298, doi:10.1175/1520-0442(1996)009<1288:
548 PPIITD>2.0.CO;2.

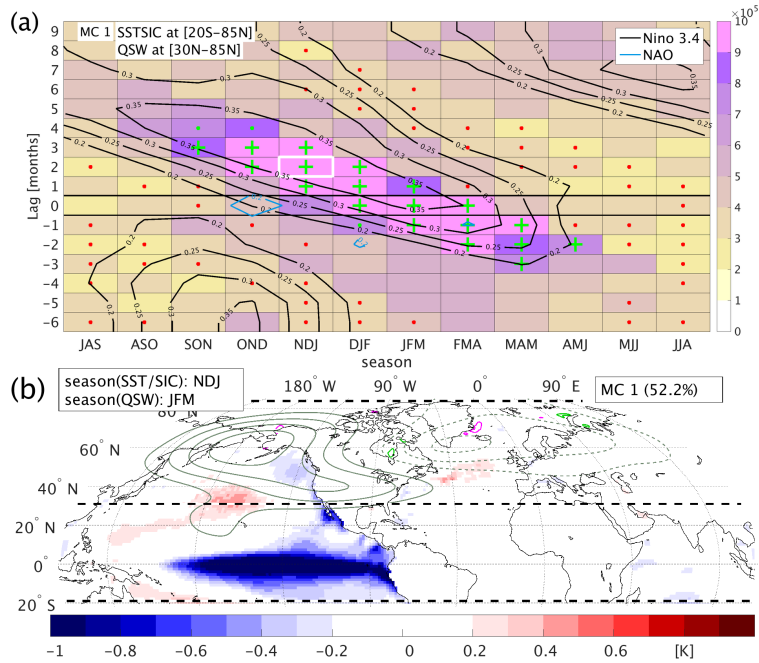
549 Visbeck, M., E. P. Chassignet, R. G. Curry, T. L. Delworth, R. R. Dickson, and G. Krahnmann,
550 2003: *The Ocean's Response to North Atlantic Oscillation Variability*, 113–145. American Geo-
551 physical Union (AGU), doi:10.1029/134GM06.

- 552 Wolf, G., D. J. Brayshaw, N. P. Klingaman, and A. Czaja, 2018a: Envelope field of northern
553 hemispheric upper tropospheric (300 hpa) quasi-stationary waves (june 1979 to august 2015).
554 *Centre for Environmental Data Analysis*, doi:10.5285/c0c7998800414e46b6823dc75751bb4c.
- 555 Wolf, G., D. J. Brayshaw, N. P. Klingaman, and A. Czaja, 2018b: Quasi-stationary waves and
556 their impact on european weather and extreme events. *Quart. J. Roy. Meteor. Soc.*, **144** (717),
557 2431–2448, doi:10.1002/qj.3310.
- 558 Wu, B., R. Zhang, R. D’Arrigo, and J. Su, 2013: On the relationship between winter sea ice
559 and summer atmospheric circulation over eurasia. *J. Climate*, **26** (15), 5523–5536, doi:10.1175/
560 JCLI-D-12-00524.1.
- 561 Zimin, A. V., I. Szunyogh, D. Patil, B. R. Hunt, and E. Ott, 2003: Extracting envelopes of rossby
562 wave packets. *Mon. Wea. Rev.*, **131** (5), 1011–1017, doi:10.1175/1520-0493(2003)131<1011:
563 EEORWP>2.0.CO;2.

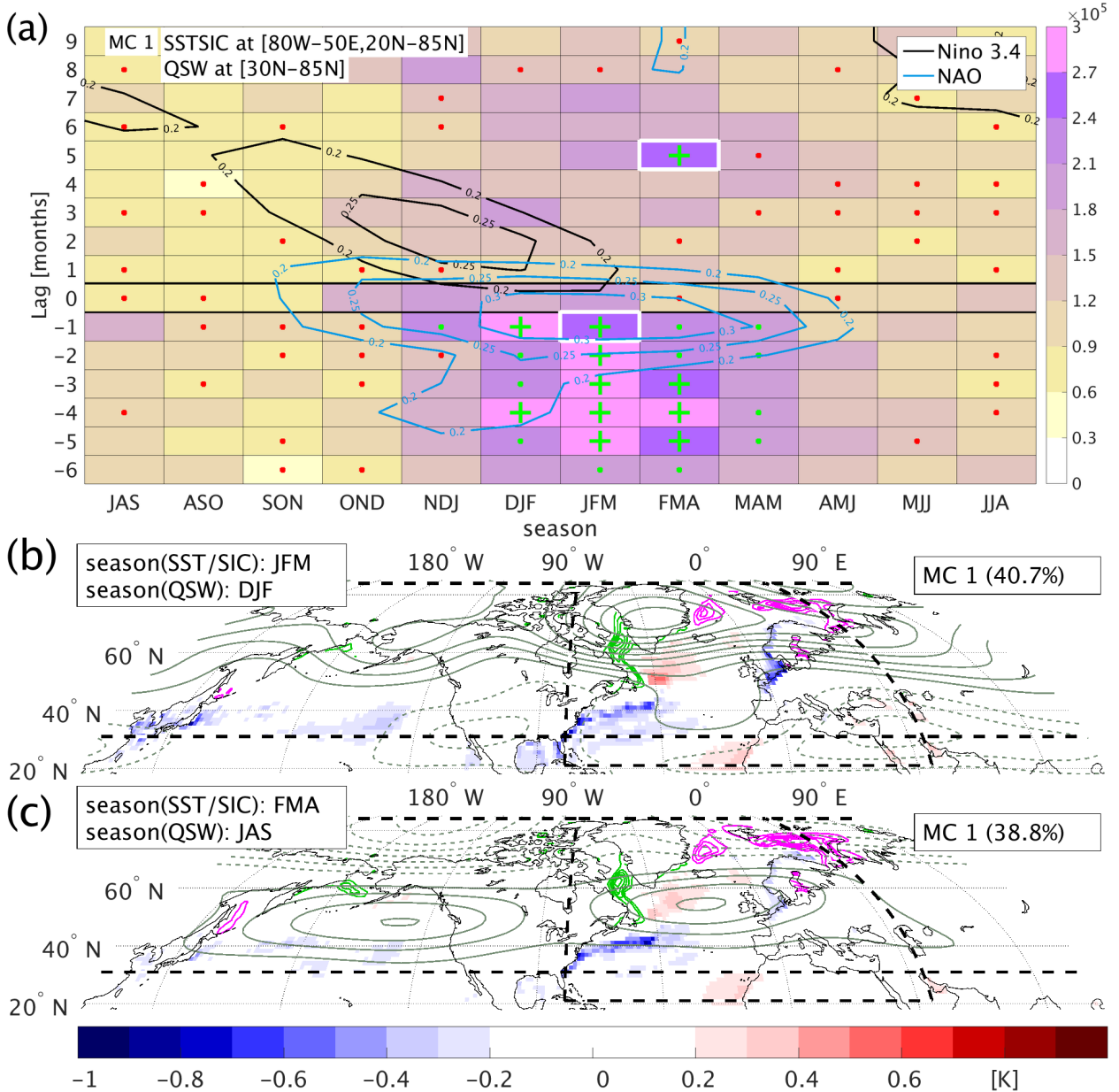
564 **6. Figures**

565 **LIST OF FIGURES**

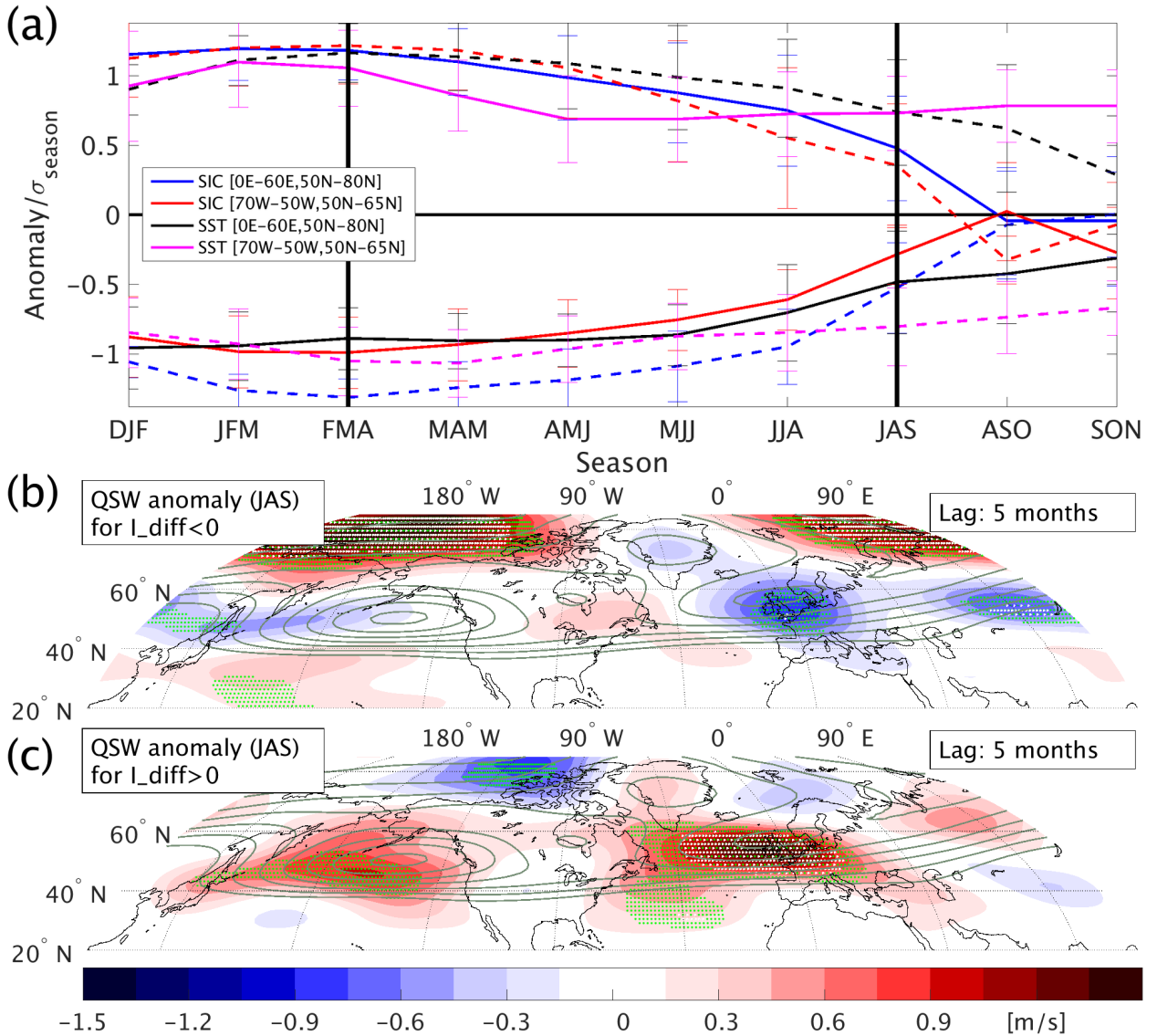
- 566 **Fig. 1.** Panel (a) shows the first MC mode for the lagged covariance matrix between extended
 567 Northern Hemisphere (20°S to 85°N) SSTSIC and extratropical Northern Hemisphere
 568 (30°N to 85°N) QSW anomalies. Shading represents covariance between associated anom-
 569 alies, weighted by their respective seasonal standard deviation. Seasons for the SSTSIC fields
 570 are given in panel (a) on the x-axis and are represented by the initial letters of the associated
 571 months. For the seasonally averaged QSW amplitudes a lag of -6 to +9 months is applied
 572 (given on the y-axis); positive lags therefore mean that the SSTSIC is leading QSW. Green
 573 plusses (dots) show statistical significant covariances based on 95th (90th) percentile. Red
 574 dots show those instances when the MC mode is not separable from the following mode,
 575 following the rule of thumb of North et al. (1982). Additional contour lines represent corre-
 576 lations between one of two global pattern indices (Niño 3.4 in black and NAO in blue) and
 577 the lagged QSW MC mode.
 578 Panel (b) shows the associated latitude-longitude pattern for the box, marked by the white
 579 edges in panel (a), for NDJ SSTSIC and JFM QSW (lag of +2 months). Boundaries for
 580 the regions used in the MC analysis are given by the black dashed lines. Shading shows
 581 anomalies of SST. Gray solid (dashed) contour lines show positive (negative) anomalies of
 582 QSW amplitude, spaced every 0.5 m/s omitting the zero contour line. Magenta (positive
 583 values) and green (negative values) contour lines show anomalies in SIC, spaced every 0.04
 584 omitting the zero contour line. All variables shown are calculated via the projection of this
 585 variable onto the timeseries of the first principal component. 28
- 586 **Fig. 2.** First MC mode between Atlantic (80°W to 50°E and 20°N to 85°N) SSTSIC and extrat-
 587 ropical Northern Hemisphere (30°N to 85°N) lagged QSW anomalies (boundaries of these
 588 regions shown by black dashed lines in panel (b) and (c)). Panel (b) and (c) show the asso-
 589 ciated latitude-longitude pattern for the boxes, marked by the white edges in panel (a), for
 590 JFM SSTSIC and DJF QSW (panel b, lag -1 month) and for FMA SSTSIC and JAS QSW
 591 (panel c, lag +5 months). Gray solid (dashed) contour lines show positive (negative) anom-
 592 alies of QSW amplitude, spaced every 0.25 m/s omitting the zero contour line. Description
 593 for all other shadings, contours, etc. are the same as in Fig. 1. 29
- 594 **Fig. 3.** Panel a shows SST and SIC persistence for a composite of the 8 years with the strongest
 595 positive and negative I_{diff} values in FMA. I_{diff} represents the difference of SIC box averages
 596 between the Labrador Sea (70°W to 50°W, 50°N to 65°N) and Greenland-Barents Sea (0°E
 597 to 60°E, 50°N to 80°N). Blue and black lines show the averaged values of SST and SIC
 598 in the Greenland-Barents Sea; red and magenta lines show the averaged values of SSTSIC
 599 in the Labrador Sea. Values associated with positive (negative) values of I_{diff} are given by
 600 solid (dashed) lines. All values are seasonally detrended and normalized by the associated
 601 seasonal standard deviation. Panel b (panel c) shows the associated anomalous QSW am-
 602 plitudes in JAS for the same composite years with $I_{\text{diff}} < 0$ ($I_{\text{diff}} > 0$). Statistical significance
 603 above the 95th (99th) percentile is given by the green (white) dots. Mean QSW amplitudes
 604 are given by the contour lines, spaced every 0.75 m/s, starting at 7.5 m/s. 30



605 FIG. 1. **Panel (a)** shows the first MC mode for the lagged covariance matrix between extended Northern
 606 Hemisphere (20°S to 85°N) SSTSIC and extratropical Northern Hemisphere (30°N to 85°N) QSW anomalies.
 607 Shading represents covariance between associated anomalies, weighted by their respective seasonal standard
 608 deviation. Seasons for the SSTSIC fields are given in panel (a) on the x-axis and are represented by the initial
 609 letters of the associated months. For the seasonally averaged QSW amplitudes a lag of -6 to $+9$ months is
 610 applied (given on the y-axis); positive lags therefore mean that the SSTSIC is leading QSW. Green pluses
 611 (dots) show statistical significant covariances based on 95th (90th) percentile. Red dots show those instances
 612 when the MC mode is not separable from the following mode, following the rule of thumb of North et al. (1982).
 613 Additional contour lines represent correlations between one of two global pattern indices (Niño 3.4 in black and
 614 NAO in blue) and the lagged QSW MC mode.
 615 **Panel (b)** shows the associated latitude-longitude pattern for the box, marked by the white edges in panel (a), for
 616 NDJ SSTSIC and JFM QSW (lag of $+2$ months). Boundaries for the regions used in the MC analysis are given
 617 by the black dashed lines. Shading shows anomalies of SST. Gray solid (dashed) contour lines show positive
 618 (negative) anomalies of QSW amplitude, spaced every 0.5 m/s omitting the zero contour line. Magenta (positive
 619 values) and green (negative values) contour lines show anomalies in SIC, spaced every 0.04 omitting the zero
 620 contour line. All variables shown are calculated via the projection of this variable onto the timeseries of the first
 621 principal component.



622 FIG. 2. First MC mode between Atlantic (80°W to 50°E and 20°N to 85°N) SSTSIC and extratropical
 623 Northern Hemisphere (30°N to 85°N) lagged QSW anomalies (boundaries of these regions shown by black
 624 dashed lines in panel (b) and (c)). Panel (b) and (c) show the associated latitude-longitude pattern for the boxes,
 625 marked by the white edges in panel (a), for JFM SSTSIC and DJF QSW (panel b, lag -1 month) and for FMA
 626 SSTSIC and JAS QSW (panel c, lag +5 months). Gray solid (dashed) contour lines show positive (negative)
 627 anomalies of QSW amplitude, spaced every 0.25 m/s omitting the zero contour line. Description for all other
 628 shadings, contours, etc. are the same as in Fig. 1.



629 FIG. 3. Panel a shows SST and SIC persistence for a composite of the 8 years with the strongest positive and
 630 negative I_{diff} values in FMA. I_{diff} represents the difference of SIC box averages between the Labrador Sea (70°W
 631 to 50°W, 50°N to 65°N) and Greenland-Barents Sea (0°E to 60°E, 50°N to 80°N). Blue and black lines show
 632 the averaged values of SST and SIC in the Greenland-Barents Sea; red and magenta lines show the averaged
 633 values of SST/SIC in the Labrador Sea. Values associated with positive (negative) values of I_{diff} are given by
 634 solid (dashed) lines. All values are seasonally detrended and normalized by the associated seasonal standard
 635 deviation. Panel b (panel c) shows the associated anomalous QSW amplitudes in JAS for the same composite
 636 years with $I_{\text{diff}} < 0$ ($I_{\text{diff}} > 0$). Statistical significance above the 95th (99th) percentile is given by the green (white)
 637 dots. Mean QSW amplitudes are given by the contour lines, spaced every 0.75 m/s, starting at 7.5 m/s.